Supplementary Information

Accompanying:
Filtered Backprojection for the Reconstruction of a High-Resolution (4,2)D CH_3-NH NOESY Spectrum on a 29 kDa Protein

Brian E. Coggins, Ronald A. Venters and Pei Zhou
Department of Biochemistry and Duke NMR Center
Duke University, Durham, NC 27710

Appendix: Mathematics of Filtered Backprojection

The Radon Transform. A mathematical basis for projection-reconstruction was first proposed in 1917 by Johann Radon[1]. For the purpose of simplicity and illustration, we will describe the results for 2D reconstructions from 1D projections at first, and then extend these for (4,2)D PR-NMR. The projection operation for a 2-D function $S(x, y)$ can be described by the integral transform:

$$P(r,\theta) = \mathbf{R}\,S(x,y) = \int_{-\infty}^{\infty} S(r\cos\theta - s\sin\theta, r\sin\theta + s\cos\theta)\,ds \qquad \text{(S1)}$$

which is known as the Radon Transform (denoted here by an operator **R**). Figure S1 illustrates this transform. The function $P(r, \theta)$ describes the values of points on projections. Note that the transform acts on a function in Cartesian coordinates to produce a function in polar coordinates, where the angle θ to the x axis defines a projection, and r specifies a position along that projection. The effect of this transform is to determine line integrals. Thus for a point $A(r, \theta)$, the value of the transform is determined by integrating $P(x, y)$ along a line orthogonal to the projection of angle θ, passing through point A. The variable of integration, s, denotes a position on this line of integration.

Inversion of the Radon Transform. Radon derived an analytical inversion formula for this transform[1]. Rowland[2] provides a concise representation in operator notation:

$$S = \mathbf{R}^{-1}P = \frac{-1}{2\pi}\mathbf{BHD}\,P \qquad \text{(S2)}$$

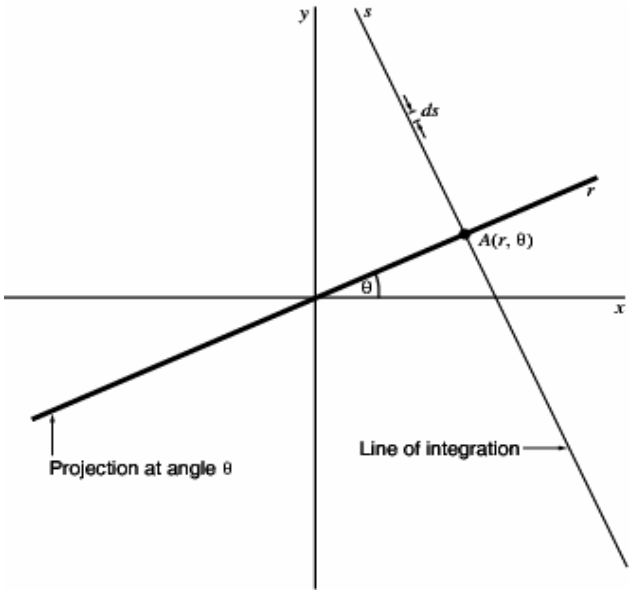

Figure S1. The Radon transform. A single projection is shown at angle θ. The value at point A is determined by integrating values of $S(x, y)$ along the line s. The complete integral transform is a 2-D function of θ and r, formed by evaluating all such lines of integration for all such projections.

where **D** is the partial differentiation operator:

$$\mathbf{D}\, g\left(r,\theta\right) = \frac{\partial g}{\partial r} \tag{S3}$$

with respect to r, **H** is the Hilbert transform operator:

$$G(r,\theta) = \mathbf{H}\, g\left(r,\theta\right) = \frac{-1}{\pi}\int \frac{g\left(u,\theta\right)}{r-u}\, du \tag{S4}$$

describing a 1-D Hilbert transform of each projection with respect to r, and **B** is the 2-D backprojection operator:

$$G\left(x,y\right) = \mathbf{B}\, g(r,\theta) = \int_0^{\pi} g\left(x\cos\theta + y\sin\theta, \theta\right) d\theta \tag{S5}$$

The inversion process can be considered as two steps, (1) a filtering step (the word "filter" being used in the signal processing sense), carried out on the projection data by the operators **D** and **H**, and (2) a backprojection step, carried out by the operator **B** on the filtered data. Reconstruction of discrete data by direct inversion of the Radon transform is often called "filtered backprojection."

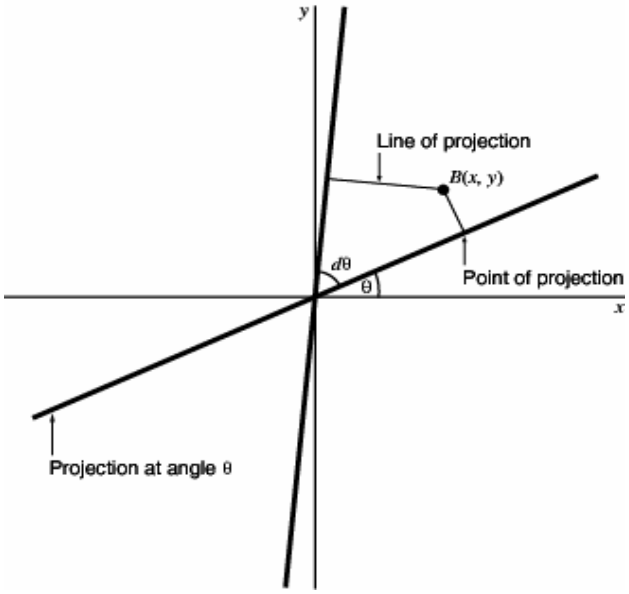

Figure S2. The backprojection operation. The value of a point, such as *B,* is determined by summing the values at the points of projections for all projections at all angles. Here are shown the contributions from two projections. The lines of projection can be followed to their intersections with the projections, and the values at these point of projection are then added.

Consider the backprojection step first, which is illustrated in Figure S2. Note that **B** acts on a function in polar coordinates to produce a function in Cartesian coordinates, reversing the coordinate system change that occurs in the Radon transform of Equation S1. In Equation S5, the integration is carried out with respect to θ, the projection angle, and therefore it should be clear that the value of G at a point $B(x, y)$ is determined by combining one value from each projection, over infinitely many projections recorded at different angles. For a single projection at angle θ, the position of the one value that is used from the projection is determined by $r = x \cos \theta + y \sin \theta$, which is, in fact, simply the point onto which B projects. Thus backprojection is equivalent to adding up the values of all points of projection. The effect of backprojection can also be understood as extending ridges of intensity out from a projection, and then adding together the ridges from all of the projections. Features emerge in the reconstruction where ridges from all of the projections intersect. When there are many projections, the heights of these features will greatly exceed the heights of the ridges. However, as we noted previously, backprojection in the limit of many projections will broaden peaks substantially[3]. Additionally, since the height of the baseline is dependent on the height of the ridges, the baseline level is substantially elevated from zero,

and shows significant fluctuations, depending on the integral of the signal intensities within the plane. Both of these factors are detrimental for the successful application to spectra, such as NOESY, that require quantitative reconstruction.

The analytical inversion of the Radon Transform, Equation S2, would correct for peak broadening and baseline distortion by applying the operators **H** and **D**. The Fourier and Radon transforms are closely related, however, and it has long been known[2] that Equation S2 can be expressed in a more computationally convenient form using the relation:

$$\mathbf{HD} = \mathbf{F}\left|t\right|\mathbf{F}^{-1} \tag{S6}$$

where **F** is the 1-D Fourier transform along the radial dimension r, $\mathbf{F}^{-1}$ is its inverse and t is the radial time domain coordinate. Thus, the inverse Radon transform can be rewritten as:

$$S = \mathbf{R}^{-1}\,P = \mathbf{BF}\left|t\right|\mathbf{F}^{-1}\,P \tag{S7}$$

which still results in the backprojection of filtered projections. In Equations 1, S6 and S7, we use **F** where the literature would use $\mathbf{F}^{-1}$ and vice versa. Most other applications of PR begin in an object domain and use a forward Fourier transform to obtain a spatial frequency domain for filtering. NMR projection data are already in the frequency domain, and thus an inverse transform returns the data to the time domain (*i.e.* equivalent to the processed FIDs). As a result, the filtering process is carried out by apodization in what would be, for NMR, the time domain. The apodization function in 2D is $|t|$, a linear function of the radial coordinate. Since multiplying two functions in the time domain is the same as convolving their Fourier transforms in the frequency domain, the effect of the time domain multiplication by $|t|$ is the same as convolving the frequency domain peaks on the projections with the function $c(r)$ = 2 sinc $2r$ - sinc^2 r, which is the Fourier transform of a linear window function with limited time domain duration[4]:

$$\mathbf{F}\left|t\right|\mathbf{F}^{-1}\,P = P * c = \int_{-\infty}^{\infty} P\left(r,\theta\right)c\left(r-u\right)du \tag{S8}$$

producing troughs of negative intensity beside each ridge of positive intensity (Figure 1, top right panel, in the main text). This suggests an equation for reconstruction in the frequency domain:

$$S = \mathbf{R}^{-1} P = \mathbf{B}\, P * c = \mathbf{B} \int_{-\infty}^{\infty} P(r,\theta) c(r-u)\, du \tag{S9}$$

When backprojected, these negative troughs (Figure 1, top right) cancel the broadening of features caused by the positive ridges. With infinitely many projections, the negative and positive ridges of the actual peaks merge together to form a new baseline centered at zero.

Equations S2, S7 and S9 are all correct expressions for the inverse Radon transform for 2D reconstructions from 1D vectors. In practice, Equation S7 is the most efficient for calculation, and is used for implementation of the FBP algorithm in the PR-CALC program. The form given in the main text, Equation 1, is a generalization of Equation S7 for arbitrary dimensionality, where *w* is understood to be the appropriate window function for the data at hand.

Of course, while the description above is for a (2,1)D case, the experiments described here are actually (4,2)D experiments. Because one dimension in a (4,2)D experiment is the directly observed proton dimension, the problem is actually the reconstruction of a 3D function from 1D vectors. It can be derived[5] that the correct filter function for a 3D reconstruction from 1D projections would be the quadratic function of the radial coordinate, t^2. Similar to the linear window function $|t|$, the t^2 filter also produces troughs around the real peaks, except that the troughs are steeper and narrower. In this case, the effect of backprojection is to extend planes perpendicular to each projection, rather than ridges. With a sufficient number of projections, the positive planes reinforce at peak positions to form peaks, while positive and negative planes cancel elsewhere in the 3D space, to give a flat baseline centered at zero.

The discussions above can be used to derive specific equations for the (4,2)D FBP NOESY experiment described in this paper. Beginning with the basic equation for FBP reconstruction, Equation 1, we can write a version with the geometry of (4,2)D PR-NMR, with spherical coordinates r, θ and ϕ for the projection data P; Cartesian coordinates x, y and z for the 4-D reconstruction S; the extra coordinate h for both, representing the directly-observed proton dimension; and the t^2 filter function described above:

$$S(x,y,z;h) = \mathbf{R}^{-1}\,P(r,\theta,\phi;h) = \mathbf{BF}\,t^2\,\mathbf{F}^{-1}\,P(r,\theta,\phi;h)$$
$$\text{with } r = x\cos\theta\sin\phi + y\sin\theta\sin\phi + z\cos\phi \text{ for any } x,y,z,\theta,\phi \tag{S10}$$

where the angle θ is measured in the *x*/*y* plane, with angle zero along *x*, and angle ϕ is measured from the *z* axis, with angle zero along the *z* axis. Over the course of the derivation we will replace the generic variables with the explicit frequency and angle variables used in this experiment. To emphasize the distinction between the directly-observed dimension, and the indirect dimensions, we have used a semicolon to separate them. The projection data are treated here as a continuous function of three spherical coordinates, plus the directly-observed coordinate *h*. In practice, they are collected as independent 2D projections with dimensions *r* and *h*, each taken at independent angles θ and ϕ, but for the discussion of the mathematics it is most convenient to consider all of them collectively. In this equation, we assume that the spherical angle space is sampled evenly, which is different from the conventional notation that θ and ϕ are sampled on a regular grid. In the latter case, an additional term, $\sin\phi$, would be needed to account for oversampling at the poles.

Substituting a 3-D version of Equation S5, the backprojection operator,

$$\begin{aligned} G(x,y,z) &= \mathbf{B}\,g(r,\theta,\phi) \\ &= \int_0^{\pi}\int_0^{\pi} g(r,\theta,\phi)\,d\theta\,d\phi \\ &\text{with } r = x\cos\theta\sin\phi + y\sin\theta\sin\phi + z\cos\phi \text{ for any } x,y,z,\theta,\phi \end{aligned} \tag{S11}$$

yields:

$$S(x,y,z;h) = \int_0^{\pi}\int_0^{\pi} \mathbf{F}\,t^2\,\mathbf{F}^{-1}\,P(r,\theta,\phi;h)\,d\theta\,d\phi$$
$$\text{with } r = x\cos\theta\sin\phi + y\sin\theta\sin\phi + z\cos\phi \text{ for any } x,y,z,\theta,\phi \tag{S12}$$

Next, the operator **F**,

$$G(s) = \mathbf{F}\,g(x) = \int_0^{\pi} g(x)\,e^{-i2\pi xs}\,dx \tag{S13}$$

is replaced with its explicit definition to give:

$$S(x,y,z;h) = \int_0^{\pi}\int_0^{\pi}\int_{-\infty}^{\infty} t^2\,\mathbf{F}^{-1}\,P(r,\theta,\phi;h)\,e^{-i2\pi rt}\,dt\,d\theta\,d\phi$$
$$\text{with } r = x\cos\theta\sin\phi + y\sin\theta\sin\phi + z\cos\phi \text{ for any } x,y,z,\theta,\phi \tag{S14}$$

When the last operator, $\mathbf{F}^{-1}$, is replaced, we have need for two different variables to describe the radial frequency coordinate. The variable r already has a specific meaning, as shown above, and we will therefore designate r' to serve as the frequency coordinate for integration in the innermost transform:

$$S(x,y,z;h) = \int_0^{\pi}\int_0^{\pi}\left[\int_{-\infty}^{\infty}\left(\int_{-\infty}^{\infty} P(r',\theta,\phi;h)\,e^{i2\pi tr'}\,dr'\right)t^2 e^{-i2\pi rt}dt\right]d\theta\,d\phi \qquad \text{with } r = x\cos\theta\sin\phi + y\sin\theta\sin\phi + z\cos\phi \text{ for any } x,y,z,\theta,\phi \tag{S15}$$

The innermost integral, in parentheses, is a 1D inverse Fourier transform with respect to the frequency domain coordinate r', transforming the data into the time domain, as a function now of the time domain coordinate t. The next further integral, enclosed in square brackets, includes the filtering operation—multiplication by t^2—as well as the forward Fourier transform that returns the data to the frequency domain, in terms of coordinate r. Using explicit notation for NMR frequency and time dimensions, with $x = \omega_{HM}$, $y = \omega_{CM}$ and $z = \omega_N$, this becomes:

$$\begin{aligned} &S(\omega_{HM},\omega_{CM},\omega_N;\omega_{HN}) \\ &\quad = \int_0^{\pi}\int_0^{\pi}\left[\int_{-\infty}^{\infty}\left(\int_{-\infty}^{\infty} P(\omega_{tilt'},\theta,\phi;\omega_{HN})\,e^{i2\pi t_{tilt}\omega_{tilt'}}\,d\omega_{tilt'}\right)t_{tilt}^2 e^{-i2\pi\omega_{tilt}t_{tilt}}dt_{tilt}\right]d\theta\,d\phi \end{aligned} \tag{S16}$$

where $\omega_{tilt} = \omega_{HM}\cos\theta\sin\phi + \omega_{CM}\sin\theta\sin\phi + \omega_N\cos\phi$ is the frequency coordinate on the tilt axis for the outer Fourier transform, and t_{tilt} and $\omega_{tilt'}$ are the time and frequency variables of integration, respectively, for the inner transforms. In practice, the filtering step is carried out first:

$$P'(\omega_{tilt},\theta,\phi;\omega_{HN}) = \int_{-\infty}^{\infty}\left(\int_{-\infty}^{\infty} P(\omega_{tilt'},\theta,\phi;\omega_{HN})\,e^{i2\pi t_{tilt}\omega_{tilt'}}\,d\omega_{tilt'}\right)t_{tilt}^2 e^{-i2\pi\omega_{tilt}t_{tilt}}dt_{tilt} \tag{S17}$$

giving filtered data P', followed by backprojection:

$$\begin{aligned} &S(\omega_{HM},\omega_{CM},\omega_N;\omega_{HN}) \\ &\quad = \int_0^{\pi}\int_0^{\pi} P'(\omega_{tilt},\theta,\phi;\omega_{HN})\,d\theta\,d\phi \\ &\quad = \int_0^{\pi}\int_0^{\pi} P'(\omega_{HM}\cos\theta\sin\phi + \omega_{CM}\sin\theta\sin\phi + \omega_N\cos\phi,\theta,\phi;\omega_{HN})\,d\theta\,d\phi \end{aligned} \tag{S18}$$

where all coordinates are now written explicitly.

The equations above are all written as continuous functions of a continuous projection data set. In reality, a finite number of projections are measured at specific angles, and discrete transforms must be used. Equations S17 and S18 can be rewritten to account for this:

$$P_i'\left(\omega_{\text{tilt}};\omega_{\text{HN}}\right)=\frac{1}{N}\sum_{j=1}^{N}\left(\sum_{k=1}^{N}P_i\left(\omega_{\text{tilt},\,k};\omega_{\text{HN}}\right)e^{i2\pi t_{\text{tilt},\,j}\omega_{\text{tilt},\,k}}\right)t_{\text{tilt},\,j}^{2}e^{-i2\pi\omega_{\text{tilt}}t_{\text{tilt},\,j}} \tag{S19}$$

$$S\left(\omega_{\text{HM}},\omega_{\text{CM}},\omega_{\text{N}};\omega_{\text{HN}}\right)\cong\sum_{i=1}^{n}P_i'\left(\omega_{\text{tilt}};\omega_{\text{HN}}\right)=\sum_{i=1}^{n}P_i'\left(\omega_{\text{HM}}\cos\alpha_{\text{HM},\,i}+\omega_{\text{CM}}\cos\alpha_{\text{CM},\,i}+\omega_{\text{N}}\cos\alpha_{\text{N},\,i};\omega_{\text{HN}}\right) \tag{S20}$$

where P_i is a given projection with projection angles $\alpha_{\text{HM},i}$, $\alpha_{\text{CM},i}$ and $\alpha_{\text{N},i}$, P_i' is a filtered projection, n is the number of projections, N is the number of data points along the tilted axis of each projection and $\omega_{\text{tilt},\,u}$ and $t_{\text{tilt},\,u}$ indicate the frequency or time coordinate, respectively, for a data point u. We prefer to describe projection directions using angles relative to each Cartesian axis, notated as $\alpha_{(axis)}$, rather than the spherical coordinate angles θ and ϕ. This practice was adopted because it is more general across spaces of different dimensionalities, and because it is more straightforward for many different calculations.

References:

(1) Radon, J. *Berichte der Sächsischen Gesellschaft der Wissenschaften, Leipzig, Math.-Phys. Kl.* **1917**, *69*, 262-277.

(2) Rowland, S. W. In *Image Reconstruction from Projections*; Herman, G. T., Ed.; Springer-Verlag: Berlin, 1979.

(3) Venters, R. A.; Coggins, B. E.; Kojetin, D.; Cavanagh, J.; Zhou, P. *J. Am. Chem. Soc.* **2005**, *127*, 8785-8795.

(4) Bracewell, R. N. *The Fourier Transform and Its Applications*; McGraw-Hill: Boston, 2000.

(5) Shepp, L. A. *Journal of Computer Assisted Tomography* **1980**, *4*, 94-107.

Comparison to Conventional 4D Experiment

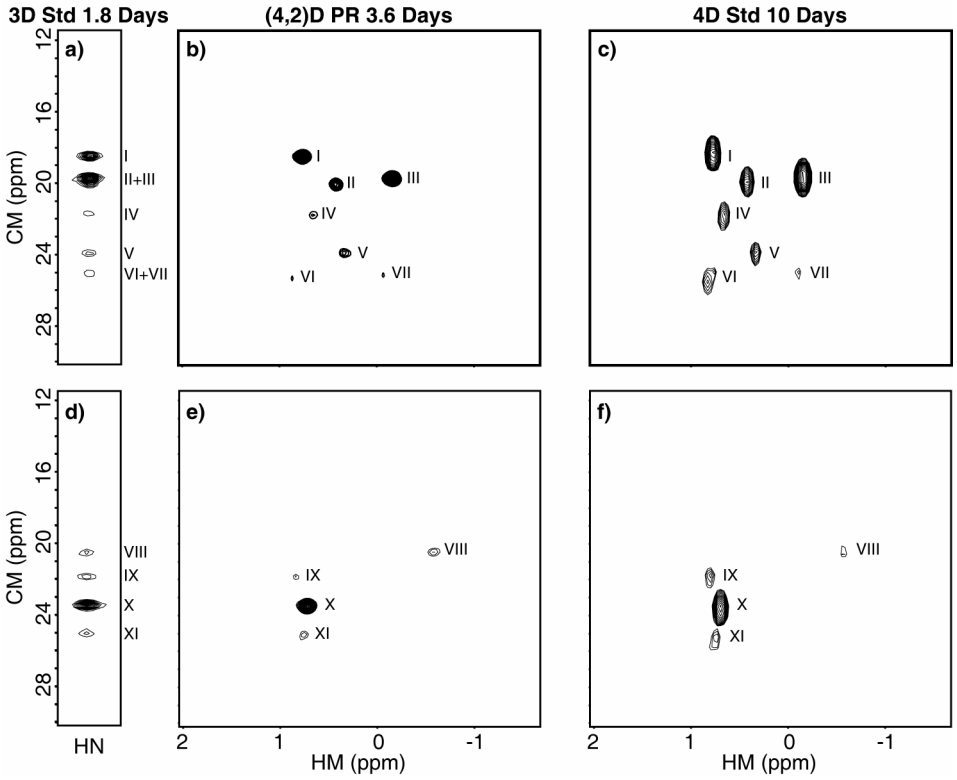

Figure S3. A comparison of the PR-NMR results with a conventional 4D NOESY spectrum, for the examples shown in the main text. Results at top are for residue S50 (HN=8.38 ppm, N=122.55 ppm), at bottom for residue C205 (HN=7.62 ppm, N=114.49 ppm). The conventional experiment was measured for 10 days on a Varian INOVA 800 MHz spectrometer with room temperature probe, with a mixing time of 175 ms, at a resolution of 50 complex points in HM, and 16 complex points in the CM and N dimensions. Because of the differences in conditions, the 4D conventional experiment is not an appropriate control for assessing the sensitivity of the PR experiment. However, the 3D conventional experiment was collected with exactly identical conditions and is the appropriate sensitivity control. The 4D experiment is useful for comparing peak positions and resolutions. For all panels, the crosspeaks are: I, V78 Hγ2; II, V49 Hγ2; III, V49 Hγ1; IV, V78 Hγ1; V, L79 Hδ1; VI, L44 Hδ1→A257 HN, from an adjacent plane; VII, L79 Hδ2; VIII, V206 Hγ2; IX, L203 Hδ2; X, V206 Hγ1; XI, L140 Hδ1. (a,d) Strips from the 3D control experiment. (b,e) Contour plots of the corresponding planes from the (4,2)D PR experiment. (c,f) Contour plots of the corresponding planes from the 4D conventional experiment. All peaks from the PR experiment are present, in the same positions. The resolution in the CM dimension is significantly enhanced in the PR experiment. There is no resolution enhancement in the HM dimension, because the conventional experiment was collected with 50 complex points resolution on this axis, which is comparable to the PR resolution in this dimension.

Data Collection Parameters for Projection and Control Data

Table S1: Projection Angles

Projection Number	Angle to HM Axis (degrees)	Angle to CM Axis (degrees)	Angle to N Axis (degrees)
1	0.00	90.00	90.00
2	90.00	0.00	90.00
3	90.00	90.00	0.00
4	66.84	30.93	70.68
5	53.08	41.56	73.65
6	73.31	51.48	43.30
7	52.89	52.07	59.46
8	24.55	86.51	65.74
9	20.08	70.19	86.86
10	31.86	63.93	76.00
11	80.13	53.43	38.32
12	81.45	84.00	10.47
13	22.51	79.76	70.18
14	60.35	58.27	46.22
15	50.18	72.19	45.21
16	79.72	75.77	17.69
17	11.58	79.00	86.43
18	28.75	73.63	67.06
19	86.55	41.02	49.19
20	79.91	23.39	69.13
21	86.57	56.50	33.72
22	43.28	46.93	86.58
23	40.00	60.25	65.88
24	73.53	79.83	19.51
25	72.22	72.70	25.23
26	86.44	18.26	72.11
27	67.14	58.29	40.81
28	46.76	86.36	43.47
29	60.31	34.23	74.54
30	42.95	72.51	52.30
31	59.59	44.95	60.47
32	73.31	30.34	65.44
33	59.86	39.14	67.51
34	55.83	35.81	80.58
35	26.02	66.25	79.99
36	53.87	86.32	36.38
37	66.19	79.07	26.49
38	47.99	43.71	80.10
39	29.84	79.98	62.22
40	86.56	78.64	11.88
41	79.88	38.29	53.55

42	59.01	79.05	33.28
43	73.81	58.91	35.93
44	79.94	30.80	61.23
45	35.78	73.05	59.55
46	41.34	66.07	58.58
47	59.64	51.41	53.40
48	79.91	61.42	30.63
49	45.90	48.91	73.18
50	86.59	48.71	41.49
51	51.11	39.09	86.68
52	79.92	45.80	45.96
53	86.53	25.75	64.52
54	67.98	86.33	22.36
55	73.19	24.26	73.03
56	64.84	27.63	79.32
57	66.44	51.03	48.18
58	55.66	65.26	44.61
59	59.16	31.08	86.50
60	70.88	65.75	31.69
61	18.57	73.83	81.10
62	44.62	79.31	47.36
63	46.19	53.33	66.11
64	10.26	85.74	80.68
65	73.14	37.19	57.97
66	24.75	71.60	74.03
67	79.40	16.68	77.28
68	75.34	86.74	15.03
69	37.30	79.61	54.65
70	17.06	86.59	73.30
71	80.56	10.61	85.22
72	40.49	51.33	79.84
73	28.00	62.25	86.56
74	52.85	46.31	66.58
75	86.26	71.21	19.19
76	60.91	86.30	29.36
77	86.55	33.38	56.85
78	39.54	86.43	50.68
79	73.88	16.49	86.62
80	73.09	44.28	50.61
81	66.40	23.90	86.41
82	51.84	79.14	40.24
83	57.48	72.00	38.32
84	38.81	56.36	72.95
85	86.30	11.19	79.45
86	66.53	37.23	62.91
87	72.07	20.73	79.95
88	34.33	67.03	65.97
89	63.15	65.18	38.07
90	53.53	58.54	52.28

91	78.70	68.41	24.64
92	46.77	59.11	58.88
93	32.13	86.53	58.10
94	35.62	54.61	86.53
95	86.48	64.10	26.17
96	66.32	44.00	55.47
97	64.83	71.95	31.75
98	33.20	58.82	79.73
99	16.50	79.55	77.37
100	48.42	65.53	51.47

For each projection, 48 complex points were recorded, with 4 transients per FID. Projection time increments and spectral windows were determined, using these angles and the dimension spectral windows of Table 2, as in Coggins et al., *J. Am. Chem. Soc.* **2004,** *126*, 1000-1001:

$$\Delta t_i = \cos\alpha_i / sw_{tilt} \tag{S21}$$

and

$$sw_{tilt} = \sum_{i=1}^{n} sw_i \cos\alpha_i \tag{S22}$$

Table S2: Parameters for the (4,2)D Experiment

Dimension	**Spectral Window (Hz)**
HM	3000
CM	3800
N	3100
HN	10999

Table S3: Parameters for the 3D Conventional Experiment

Dimension	**Spectral Window (Hz)**	**Complex Points**
N	3100	48
CM	3800	48
HN	10999	512

During the processing of the HN dimension, in both the 3D and the (4,2)D experiments, the region from 11.0 to 5.6 ppm was extracted.